A LOW-NOISE, HIGH-BANDWIDTH MAGNETICALLY-LEVITATED MOMENTUM-WHEEL FOR 3-AXIS ATTITUDE CONTROL FROM A SINGLE WHEEL

Jon Seddon and Alexandre Pechev

Surrey Space Centre, University of Surrey, Guildford, GU2 7XH, UK

ABSTRACT

This paper proposes a new concept for attitude actuation for small satellites that uses active magnetic bearings to support and tilt a spinning rotor to provide 3-axis attitude control of the satellite using a single actuator. A controlled 3D motion in the spinning rotor provides a conventional torque output about the momentum axis and a gyroscopic torque output about any direction in the plane normal to the spinning axis. Therefore, a single tilting momentum-wheel can generate torque along the three principal axes of the satellite, providing mass and power savings, or redundancy.

In this paper we present a model of, and results from the engineering model that has been built of the tilting magnetically-levitated momentum-wheel. The control loop that levitates and tilts the rotor is discussed. The 3-axis actuation of this wheel is demonstrated with simulations of the wheel fitted to the TopSat small satellite. The bandwidth and torque output of the wheel are compared with a conventional momentum wheel's. The power consumption, operation and stiffness of the magnetic bearing are discussed. The 2.5 micrometre translational and 0.1 milliradian rotational control of the wheel obtained in experiments with the engineering model are demonstrated.

1. INTRODUCTION

Active Magnetic Bearings (AMBs) are increasingly being used as they have many desirable properties compared to conventional roller or ball bearings. AMBs eliminate all contact between moving parts, preventing friction, stiction and wear. Because there is no contact there is no need for lubrication, making them especially useful for use in the vacuum of space. Because of the lack of friction the spin rate of the bearing can be increased. The lack of friction will also increase the lifetime of the bearing and reduce its sensitivity to temperature. The active control of the rotor position minimises wheel jitter and makes for a very low noise bearing. There are however some disadvantages such as an increase in the complexity of the system, and an increase in power consumption due to the electromagnets, although the spin motor power consumption is reduced because of the elimination of friction and stiction.

The use of AMBs also allows the rotor to be tilted through a small range of angles if properly designed, giving it some additional properties. A conventional output torque can be generated about the rotor's spin axis and a gyroscopic torque can be generated about any axis in the plane normal to the spin axis. The AMBs allow the rotor to be tilted at a high angular rate, generating a large gyroscopic torque. Because the axis of the gyroscopic torque can be controlled, we propose a single tilting momentum wheel that can generate an output torque about all three axes of the spacecraft. The bandwidth of the output torque is very high making it ideal for the damping of vibrations and rapid reorientation of the spacecraft, for instance in rendezvous and docking procedures.

The rotor can only be tilted through a small range of angles. The range of angles is limited by the width of the airgap between the electromagnet pole face and the rotor. A large airgap reduces the magnetic flux in the airgap and so decreases the stiffness of the bearing and increases the power consumption. Finite element simulations show that a tilt range of $\pm 3^\circ$ is feasible. Because the tilt range is small and the tilt rate is high then this gyroscopic torque can only be generated for a short time. This makes the gyroscopic torque more suitable for the damping of high frequency disturbances, or for high bandwidth small-angle manoeuvres, such as in satellite rendezvous and docking.

This paper discusses the theory behind the use of AMBs in a spacecraft momentum wheel. A mathematical model of a tilting magnetically-levitated momentum-wheel is derived. A controller to stabilise the wheel is generated and the performance and properties of the wheel are simulated and discussed.

In this paper we then present experimental data from an engineering model of the wheel that has been built. The translational position of this wheel can be controlled with an accuracy of 2.5 micrometres and the tilt angle can be controlled with an accuracy of 0.1 milliradians. The bandwidth of the wheel and controller is 176 rads^{-1} and so can counteract high frequency disturbances as predicted by the simulations. The limitation in rotational and translational position is due to the resolution of the sensors.

Proc. '13th European Space Mechanisms and Tribology Symposium – ESMATS 2009', Vienna, Austria
23–25 September 2009 (ESA SP-670, July 2009)

2. SYSTEM MODEL

Prior magnetically-levitated momentum-wheels for spacecraft have used the electrodynamic principle [1][2][3], where permanent magnets generate bias flux in the magnetic bearing and actively controlled electromagnets generate a control flux to stabilise the system. This system has the advantage of having a linear relationship between the force acting on the rotor and the applied current [4]. The alternative approach taken by the authors uses the electromagnetic principle where a purely attractive force acting on the rotor is generated by electromagnets. This approach has the benefit of being able to generate larger forces, increasing the stiffness of the bearing if required [5].

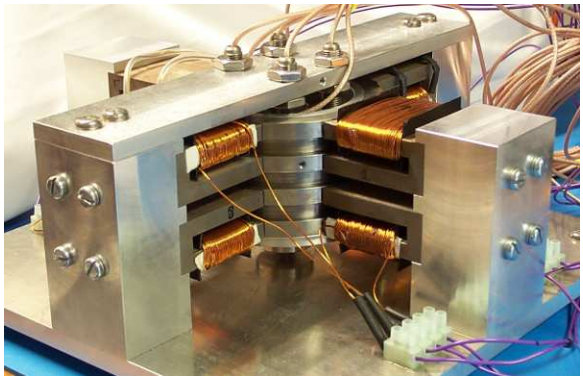

Figure 1. The engineering model of the wheel

Fig. 1 shows the arrangement of the electromagnets around the rotor in our design. The geometry of the rotor and electromagnets was optimised with the use of three-dimensional magnetostatic finite element simulations. The centre of the inertial co-ordinate system is at the geometrical centre of the rotor. x, y and z are the translational distance that the rotor has been displaced from its central position along the principal inertial axes. α_x, α_y and α_z are the angles that the rotor has been rotated about the principal inertial axes from its central position. The electromagnets are aligned along the positive and negative inertial axes.

The attractive reluctance force generated by the i-th electromagnet is given by [6]

$$f_i = -\frac{\mu_0 N^2 \varepsilon l i^2}{4\gamma^2} \tag{1}$$

where μ_0 is the permeability of free space, N is the number of terms in the electromagnet coil, εl is the cross sectional area of the electromagnet pole face, i is the current flowing through the coils and γ is the width of the airgap between the electromagnet pole face and the rotor pole face. The negative sign is to indicate that the reluctance force is attractive. The kinematics to map the force generated by each of the electromagnets to the total force acting on the rotor are

$$\begin{bmatrix} F_x \\ F_y \\ F_z \end{bmatrix} = \begin{bmatrix} 1 & 1 & 0 & 0 & -1 & -1 & 0 & 0 \\ 0 & 0 & 1 & 1 & 0 & 0 & -1 & -1 \\ 0 & 0 & 0 & 0 & 0 & 0 & 0 & 0 \end{bmatrix} \begin{bmatrix} f_1 \\ f_2 \\ f_3 \\ f_4 \\ f_5 \\ f_6 \\ f_7 \\ f_8 \end{bmatrix} \tag{2}$$

where $F = [F_x F_y F_z]^T$ is the force acting on the rotor along the principal inertial axes and f_1 to f_8 are the attractive forces generated by the eight electromagnets. The kinematic mapping between electromagnet forces and the torque on the rotor is given by

$$\begin{bmatrix} T_x \\ T_y \\ T_z \end{bmatrix} = r_z \begin{bmatrix} 0 & 0 & -1 & 1 & 0 & 0 & 1 & -1 \\ 1 & -1 & 0 & 0 & -1 & 1 & 0 & 0 \\ 0 & 0 & 0 & 0 & 0 & 0 & 0 & 0 \end{bmatrix} \begin{bmatrix} f_1 \\ f_2 \\ f_3 \\ f_4 \\ f_5 \\ f_6 \\ f_7 \\ f_8 \end{bmatrix} \tag{3}$$

where $T = [T_x T_y T_z]^T$ is the torque acting about the three principal inertial axes and r_z is the length of the moment that the torques act about, which is the distance along the z-axis from the centre of the axes to the centre of the electromagnets.

The translational dynamic behaviour of the rotor is given by Newton's Second Law

$$ma = F \tag{4}$$

where F is the vector force acting on the rotor in the inertial reference frame and a is the acceleration of the rotor in the inertial reference frame. The rotational dynamics of the rotor are given by [7]

$$I\ddot{\alpha} + \dot{\alpha} \times I\dot{\alpha} = T + T_d \tag{5}$$

where T is the control torque acting on the rotor, T_d is the disturbance torque on the rotor, I is the inertia matrix of the rotor, $\dot{\alpha}$ is the angular velocity of the rotor about the principal axes and $\ddot{\alpha}$ is the angular acceleration of the rotor about the principal axes.

Eq. 1 shows that the reluctance force generated by each electromagnet depends upon the width of the airgap of each electromagnet. This airgap depends upon the translational and rotational position of the rotor. Because of the small range considered, using small angle approximations and considering translation and rotation separately,

the change in the airgap at each electromagnet can be calculated as

$$\begin{bmatrix} \triangle\gamma_1 \\ \triangle\gamma_2 \\ \triangle\gamma_3 \\ \triangle\gamma_4 \\ \triangle\gamma_5 \\ \triangle\gamma_6 \\ \triangle\gamma_7 \\ \triangle\gamma_8 \end{bmatrix} = \begin{bmatrix} -1 & 0 & 0 & -r_z \\ -1 & 0 & 0 & r_z \\ 0 & -1 & r_z & 0 \\ 0 & -1 & -r_z & 0 \\ 1 & 0 & 0 & r_z \\ 1 & 0 & 0 & -r_z \\ 0 & 1 & -r_z & 0 \\ 0 & 1 & r_z & 0 \end{bmatrix} \begin{bmatrix} x \\ y \\ \alpha_x \\ \alpha_y \end{bmatrix} \quad (6)$$

where $\triangle\gamma_1$ to $\triangle\gamma_8$ are the changes in the airgaps at the electromagnets. The airgap width with the rotor in its central position is γ_0 and so $\gamma_i = \gamma_0 + \triangle\gamma_i$.

The dynamics of the brushless DC motor spinning the rotor are approximated in the Laplace domain by

$$\ddot{\alpha_z}(s) = \frac{si_{drive}(s)}{sK_l + K_D} \quad (7)$$

where i_{drive} is the drive current to the motor, and the inertia and damping gains K_l and K_D are taken for a typical brushless DC motor used in the laboratory, with values 1.07×10^{-2} and 0.1 respectively. The angular acceleration output by the motor is multiplied by the moment of inertia about the z-axis of the rotor (I_{zz} in the inertia matrix) to give the output torque of the spin axis motor. This output torque is added to the torque from the kinematic Eq. 3 to give the total force acting on the rotor in Eq. 5 of the rotational dynamics.

2.1. 3-axis Torque Output From the Proposed New Wheel

The 3-axis output torque from the full wheel system T is the sum of the gyroscopic output torque from tilting the wheel T' and the conventional torque from changing the angular velocity of the spinning wheel T''. Because the rotor is only tilted through a small range of angles, we can use small angle approximations to say that there is no component of the gyroscopic torque about the z-axis and the conventional acceleration torque only has a component about the z-axis.

The output torque from tilting the rotor is generated by the same physical process as a Control Moment Gyro (CMG). Incorporating the small angle approximations mentioned above, it is given by

$$T' = \begin{bmatrix} \dot{\alpha}_x \\ \dot{\alpha}_y \\ 0 \end{bmatrix} \times h_0(\alpha_x, \alpha_y, \dot{\alpha}_z) \quad (8)$$

where h_0 is the angular momentum of the spinning rotor, and is a function of the rotor spin rate about the z-axis and the angle of the rotor about the x and y axes. The angular momentum when the rotor is not tilted is

$$H_0(\dot{\alpha}_z) = I \begin{bmatrix} 0 \\ 0 \\ \dot{\alpha}_z \end{bmatrix} \quad (9)$$

The rotation matrix to rotate $H_0(\dot{\alpha}_z)$ about the y-axis and then the x-axis can be calculated by

$$\begin{aligned} R_{xy} &= \begin{bmatrix} 1 & 0 & 0 \\ 0 & \cos\alpha_x & -\sin\alpha_x \\ 0 & \sin\alpha_x & \cos\alpha_x \end{bmatrix} \begin{bmatrix} \cos\alpha_y & 0 & \sin\alpha_y \\ 0 & 1 & 0 \\ -\sin\alpha_y & 0 & \cos\alpha_y \end{bmatrix} \\ &= \begin{bmatrix} \cos\alpha_y & 0 & \sin\alpha_y \\ \sin\alpha_x\sin\alpha_y & \cos\alpha_x & -\sin\alpha_x\cos\alpha_y \\ -\cos\alpha_x\sin\alpha_y & \sin\alpha_x & \cos\alpha_x\cos\alpha_y \end{bmatrix} \quad (10) \end{aligned}$$

Therefore the output torque from tilting the rotor is given by

$$T' = \begin{bmatrix} \dot{\alpha}_x \\ \dot{\alpha}_y \\ 0 \end{bmatrix} \times R_{xy} I \begin{bmatrix} 0 \\ 0 \\ \dot{\alpha}_z \end{bmatrix} \quad (11)$$

The output torque about the z-axis from the acceleration of the rotor is given by

$$T'' = I_{zz} \begin{bmatrix} 0 \\ 0 \\ \ddot{\alpha}_z \end{bmatrix} \quad (12)$$

The output torque from the tilting magnetically-levitated momentum-wheel is the sum of the torques from tilting and accelerating the rotor $T = T' + T''$.

The spacecraft is simulated using the model described in [8]. The spacecraft inertia matrix used was from the TopSat 120 kg small satellite built by Surrey Satellite Technology Ltd.

3. CONTROLLER

For the control of a spacecraft using a single tilting magnetically-levitated momentum-wheel, we propose a two stage controller. The first outer controller calculates the necessary tilt axis and tilt angle from the commanded input torque. The second stage is a feedback controller to maintain the rotor at the desired tilt angle and spin rate.

To calculate the tilt angle required to generate the torque command demanded from the wheel, the gyroscopic output torque Eq. 8 can be rearranged to calculate the desired tilt rate from the demanded torque. Using small angle

approximations, components of the tilt torque about the z-axis are zero and the tilt rate commands are

$$\begin{bmatrix} \hat{\dot{\alpha}}_x \\ \hat{\dot{\alpha}}_x \end{bmatrix} = \frac{1}{I_{zz}\dot{\alpha}_z \cos\alpha_x \cos\alpha_y} \begin{bmatrix} 0 & -1 \\ 1 & 0 \end{bmatrix} \begin{bmatrix} \hat{T}_x \\ \hat{T}_y \end{bmatrix} \tag{13}$$

where $\hat{T}_x$ and $\hat{T}_y$ are the commanded torques about the x and y axes respectively and $\hat{\dot{\alpha}}_x$ and $\hat{\dot{\alpha}}_y$ are the desired tilt rates, which can be integrated to give the desired tilt angles. The commanded tilt torque is derived from the spacecraft attitude control loop with feedback from the quaternion error and angular body rates [8]. The input to the motor to control the spin rate of the wheel is the commanded torque about the z-axis with saturation limits applied.

The simplest form of the inner controller decouples the translational and rotational motion of the rotor and has a separate controller for each. This assumption is only valid for the derivation of the controller. The same eight electromagnets are controlling both the rotation and translation of the rotor. Any imbalance in the wheel will also couple these motions. The decoupling between rotation and translation in the final wheel should be measured.

First the Taylor series expansion of the magnitude of the reluctance force is found, ignoring higher order terms, to linearise the system

$$\begin{aligned} F_R &= \frac{\mu_0 N^2 \epsilon l i_0^2}{4\gamma_0^2} + \frac{\mu_0 N^2 \epsilon l i_0}{2\gamma_0^2}\triangle i - \frac{\mu_0 N^2 \epsilon l i_0^2}{2\gamma_0^3}\triangle\gamma \\ &= f_0 + K_i \triangle i - K_\gamma \triangle\gamma \end{aligned} \tag{14}$$

The translational force on the rotor along the x-axis is

$$\begin{aligned} F_x &= f_1 + f_2 - f_5 - f_6 \\ &= 4K_i\triangle i_x + 4K_\gamma \triangle x \end{aligned} \tag{15}$$

Using Newton's Second Law and applying the Laplace Transform, we have the transfer function

$$G_x(s) = \frac{X(s)}{i_x(s)} = \frac{4K_i/M}{s^2 - 4K_\gamma/M} \tag{16}$$

Similarly, for rotation about the y-axis

$$\begin{aligned} T_y &= r_z(f_1 + f_6 - f_2 - f_5) \\ &= 4r_z K_i \triangle i_{\alpha y} + 4r_z^2 K_\gamma \triangle \alpha_y \end{aligned} \tag{17}$$

and assuming the rotor's inertia matrix is diagonal

$$G_{\alpha y}(s) = \frac{A_y(s)}{i_{\alpha y}(s)} = \frac{4r_z K_i/I_{yy}}{s^2 - 4r_z^2 K_\gamma/I_{yy}} \tag{18}$$

The transfer functions for rotation and translation are both double integrators in the range of frequencies of interest with a constant phase angle of $-180°$. The desired response chosen for the inner controller was $55°$ of phase margin at a crossover frequency of 100 rads^{-1}. The controller was therefore made from a lead-lag compensator of the form below to generate this phase margin

$$K(s) = K\frac{s+z}{s+p}\frac{s+\omega_i}{\omega_i s} \tag{19}$$

where z and p are the zero and pole of the lead term respectively, and $p > z$. ω_i is the corner frequency of the lag term and K is the loop gain. These terms were tuned to give the desired crossover frequency and the maximum phase margin at this frequency. The crossover frequency was initially chosen to be 100 rads^{-1} for the simulations presented here.

A similar compensator can be derived for the rotational motion. The error between the desired and measured translation or rotation is fed to the input of the compensator and the output is the $\triangle i$ for motion along or about that axis. The current to electromagnet 1 is given below and the currents for the other electromagnets can be derived similarly.

$$i_1 = i_0 + i_x + i_{\alpha y} \tag{20}$$

From Eqs. 15, 17 and 20, for every translation or rotation movement there will be an increase in the current through one electromagnet and an equal decrease in the current through another electromagnet. These will cancel and so therefore, the total current for all eight electromagnets at all times with this decoupled controller is eight times the bias current.

3.1. Gyroscopic Coupling

Because of the $\dot{\alpha} \times I\dot{\alpha}$ term in the rotational dynamics of the rotor in Eq. 5 there will be a rotational disturbance on the rotor about the axis normal to the tilt and spin axes. The controller will be unable to damp this rotational disturbance when the angular velocity of the spinning wheel exceeds the system's bandwidth. A rotation of 5000 rpm has an angular frequency of 524 rads^{-1}, which will exceed the bandwidth of the system and the wheel will be unstable.

This rotational disturbance can be cancelled using feedback linearisation via a feed forward compensator. The torque required to cancel the $\dot{\alpha} \times I\dot{\alpha}$ disturbance can be

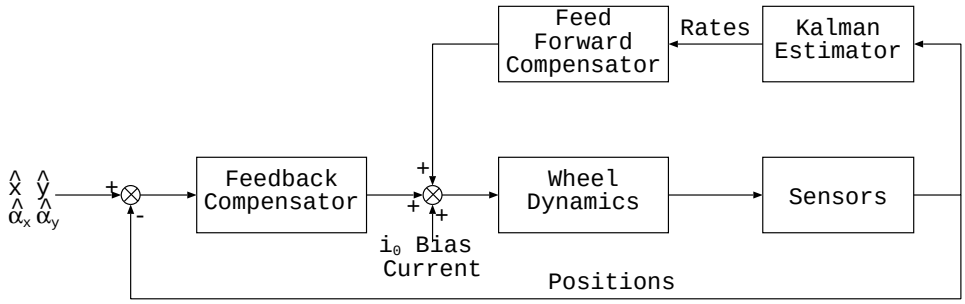

Figure 2. A block diagram of the final system

calculated. The force required at each electromagnet to generate this torque is calculated using the system's kinematics. The current required to generate this force is then added to the current demand to each electromagnet from the feedback lead-lag compensator. Fig. 2 shows a block diagram of the complete system including the feed forward compensator.

The sensors in the system measure the position of the rotor; a Kalman estimator has been built to calculate the angular rate $\dot{\alpha}$ about the two tilt axes from the sensors' outputs. The brushless DC motor contains Hall sensors that allow the angular velocity of the rotor about its spin axis to be calculated.

Without the feed forward current being added to the current from the controller, when a rotation of the rotor about the x-axis is demanded, the lead-lag compensator drives electromagnets 3, 4, 7 and 8 to tilt the wheel and 1, 2, 5 and 6 to cancel the gyroscopic disturbance. The rotor becomes uncontrollable when its spin angular velocity exceeds the system's crossover frequency. After the addition of the feed forward term, the wheel is stable at all angular velocities, and for rotations of the rotor about the x-axis the lead-lag compensator outputs only the bias current i_0 for electromagnets 1, 2, 5 and 6.

In the hardware implementation, a discrete-time solver is used to implement the controller and feed forward gain. Our hardware set-up implements control loops on a PC running a real-time operating system, with a time step period of 1 ms. With this sampling frequency, the implementation of the feed forward gain will limit the maximum angular velocity of the spinning rotor.

3.2. Mass Imbalance

There are two types of mass imbalance in a spinning rotor. Static imbalance due to an offset between the centre of mass and the centre of rotation. Dynamic imbalance due to the principle axes of inertia being rotated from the geometrical axes. These imbalances exert a translational disturbance force and rotational disturbance torque on the rotor respectively. Because the inertia matrix is calculated about the rotor's principle geometric axes, a dynamic imbalance causes the rotor's inertia matrix to be non-diagonal [9]. Therefore the feed forward term proposed will cancel the disturbance caused by the dynamic imbalance of the wheel, resulting in a lower output noise from a tilting magnetically-levitated momentum wheel.

If the rotor cannot be balanced to a high enough static imbalance tolerance, then an additional feed forward loop to cancel translational disturbances can be added.

3.3. Torque Transfer

The output torque generated when the wheel is tilted is generated by the same physical process as a Control Moment Gyro (CMG), and is given by Eq. 11. The vector cross product term in this equation means that the output torque axis is perpendicular to the tilt axis. In a CMG the output torque is transferred to the spacecraft by the mechanical bearings. In a tilting magnetically-levitated momentum-wheel the torque is transferred by the electromagnets. The feed forward term presented in Section 3.1 will generate the stiffness required to transfer this torque. The maximum current that can be supplied to each electromagnet will determine the maximum torque that can be transferred to the spacecraft.

4. RESULTS

4.1. Simulation Results

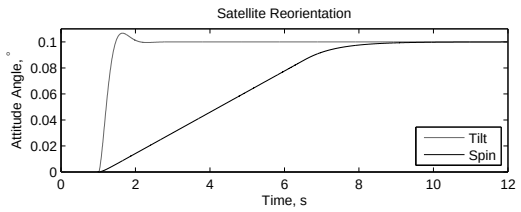

Figure 3. The satellite's attitude when reorientating using a tilting momentum wheel and a conventional momentum wheel, with the conventional torque limited to a maximum value

Fig. 3 shows the attitude of the TopSat spacecraft when it was reorientated through 0.1° by tilting the momen-

tum wheel and also by conventionally accelerating the spinning rotor. Because of the larger output torque available from tilting the wheel, this reorientation can be performed almost five times faster than is possible by operating the wheel conventionally. The axis of the output torque when tilting the wheel is not fixed and so this torque can be generated about any axis normal to the wheel's spin axis.

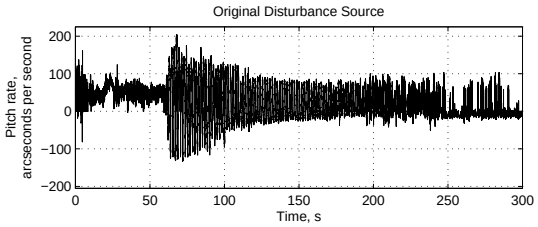

Figure 4. The attitude rate observed on the UK-DMC satellite while it was suffering from a high frequency disturbance [10]

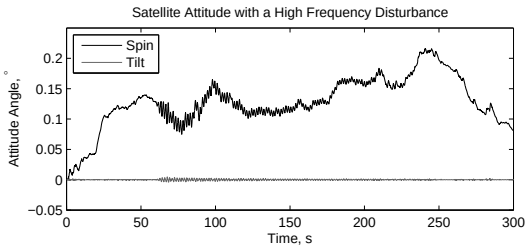

Figure 5. The satellite's attitude when applied with a high frequency disturbance torque that is being damped by a tilting momentum wheel and a conventional momentum wheel

A disturbance in the attitude rates of the UK-DMC spacecraft was identified through image processing [10]. With a frequency of 0.6 Hz the disturbance was too high for the conventional momentum wheels on UK-DMC to damp. The effect of the disturbance is visible in the attitude rate shown in Fig. 4. This angular rate data was differentiated to give an angular acceleration and then multiplied by UK-DMC's moment of inertia about that axis to give the torque that caused the disturbance. This torque was then applied to the TopSat model and its attitude is shown in Fig. 5 when the disturbance is damped by the momentum wheel operating conventionally and when tilting.

The magnitude of the attitude disturbance is over twenty times less when damped with a tilting momentum-wheel than when it is damped by a momentum wheel operating conventionally. This improvement in performance is due to the tilting momentum-wheel's improved bandwidth.

The disturbance was applied about the x-axis of the spacecraft. Fig. 6 shows the current through two electromagnet coils when damping the high-frequency disturbance torque. Because of the gyroscopic nature of the output torque from tilting the rotor, the rotor must be tilted about the y-axis to counteract the disturbance

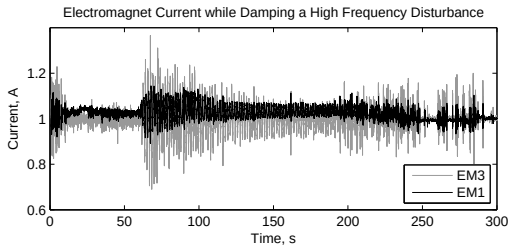

Figure 6. The current in two electromagnets when damping a high frequency disturbance torque

about the x-axis. Electromagnet 1 is one of the four magnets that controls the tilt of the wheel about the y-axis. The varying current in electromagnet 3 is due to the current required by the feed forward term in the controller. This feed forward term prevents any gyroscopic motion of the rotor. Preventing the gyroscopic motion of the rotor transfers the gyroscopic torque produced to the spacecraft to generate the tilting component of the output torque T'.

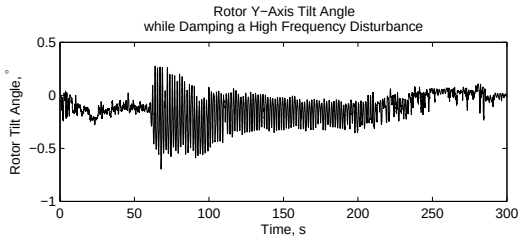

Figure 7. The rotor tilt angle when damping a high frequency disturbance torque

Fig. 7 shows how the tilt angle of the rotor about the y-axis varies as the earlier disturbance torque is damped.

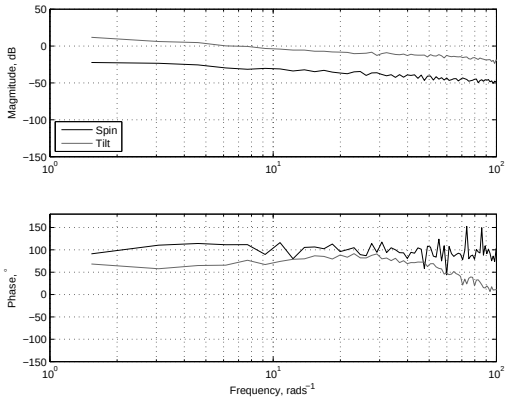

Figure 8. The frequency response of a tilting and a conventional momentum wheel

The frequency response of the entire spacecraft attitude when controlled using a tilting momentum-wheel and a conventional momentum-wheel was measured using a Dynamic System Analysis (DSA) tool developed by the authors. A white-noise disturbance was injected into

the attitude control loop and the system's response was recorded. The bode plot of the response is shown in Fig. 8. When controlled with the tilting momentum wheel the crossover frequency of the system is at 6 rads^{-1}. The crossover frequency of the conventional wheel system is two orders of magnitude less.

4.2. Experimental Results

An engineering model of the wheel has been built and is currently being tested to verify its simulated properties and to allow the development of controllers. The results presented in this section are the initial results from this testing. Fig. 1 shows a photograph of the wheel. The stator electromagnets are built from laminated steel with a curved pole face accurately cut using wire erosion. The position and tilt angle of the wheel is measured by contact free eddy current sensors, which measure the position of an aluminium liner inside the steel rotor to an accuracy of 2 μm. Low noise current amplifiers were built from linear audio amplifier ICs. The controller was implemented on a PC running a real time operating system sampling at 1 kHz.

The frequency response of the amplifier and electromagnets was measured using the DSA tool. The measured response was combined with the numerical model of the translation and rotation dynamics and the anti-aliasing filters, to derive a controller. The controller variables were adjusted to give the maximum phase margin at the system's crossover frequency.

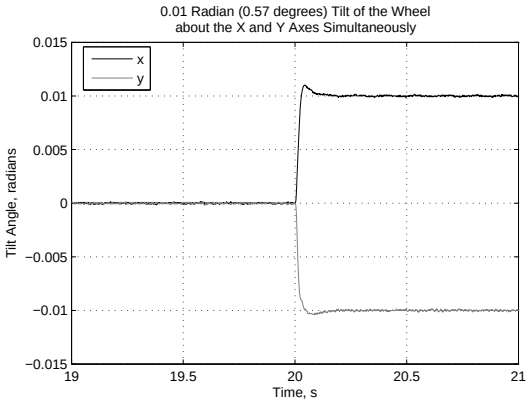

Figure 9. A rotation step response with the axis of rotation between the wheel's principle axes

Fig. 9 shows the response of the wheel to a step command for a rotation about an axis between the wheel's x and y principle axes. The electromagnets are aligned with the x and y principle axes. This plot demonstrates that it is possible to tilt the wheel about any axis on the plane normal to the wheel's spin axis and therefore to generate a torque about any axis on this plane. Experiments show that the translation loop is decoupled from the rotation loop by at least -46 dB up to the crossover frequency.

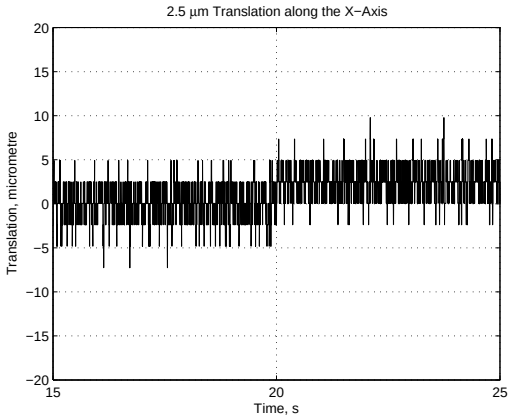

Figure 10. The response to a 2.5 micrometre translation step command along the x-axis

Fig. 10 shows the wheel's response to the step command for a 2.5 micrometre translation along the positive x-axis at time 20.0 seconds. The data acquisition card used in the engineering model has a 12-bit resolution, with the least significant bit corresponding to a translation of 2.4 μm. The quantisation of the position is visible showing that the wheel can be controlled with a very high precision, with the engineering model's precision being limited by the resolution of the data acquisition card.

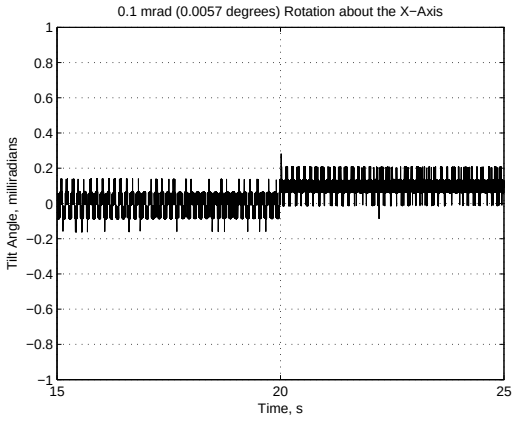

Figure 11. The response to a 0.1 milliradian rotation step command about the x-axis

Fig. 11 shows the wheel's response to the step command for a 0.1 milliradian (0.0057°) rotation about the x-axis. Again the resolution of the 12-bit data acquisition card is defining the resolution that the wheel can be tilted with.

Fig. 12 shows the measured and simulated frequency response of the loop transfer function of the initial decoupled rotation controller and plant dynamics. The simulated model gives a good phase match at lower frequencies. The cross over frequency of the measured system is 176 rads^{-1} with a phase margin of 28°.

The wheel can be tilted at a rate of 1.0 rads^{-1} allowing

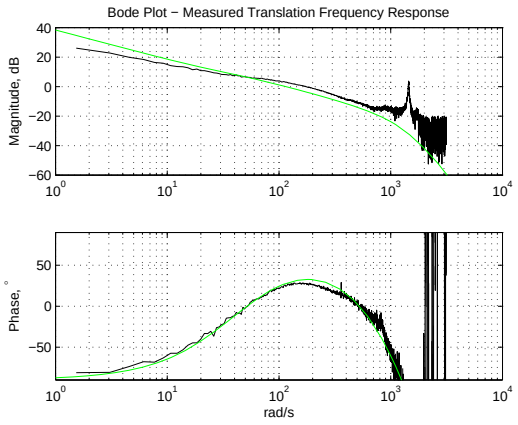

Figure 12. The measured (black) and simulated (green) frequency response of the loop transfer function of the decoupled translation controller and dynamics

a gyroscopic torque of 1.2 Nm to be generated. The tilt rate is determined by the speed of the controller. The controller can be made faster. Increasing the tilt rate will allow the same magnitude of gyroscopic torque to be generated with the wheel spinning at lower rates.

5. CONCLUSION

We propose a novel concept for 3-axis attitude control of a spacecraft using a single momentum wheel that uses an active magnetic bearing. Using an active magnetic bearing allows a momentum wheel for spacecraft attitude control to be made with improved properties compared to a wheel that uses conventional bearings. The use of active magnetic bearings allows a single wheel to generate an output torque about all three axes of the spacecraft. A conventional output torque can be generated about the spin axis of the wheel and a gyroscopic torque can be generated about any axis on the plane normal to the spin axis. Because the gyroscopic torque is generated by tilting the wheel it has a high bandwidth, and because its magnitude is proportional to the tilt rate its magnitude can be high. The ability to tilt the wheel allows for the cancellation of mass imbalances, providing very low noise actuation. The simulated properties of the wheel have been successfully demonstrated by the engineering model of the wheel that has been built.

ACKNOWLEDGEMENTS

The authors would like to thank The Nuffield Foundation for their partial support of this project with grant NAL/32791.

REFERENCES

[1] Murakami, C., Ohkami, Y., Okamoto, O., Nakajima, A., Inoue, M., Tsuchiya, J., Yabu-Uchi, K., Akishita, S. & Kida, T. (1984). A New Type of Magnetic Gimballed Momentum Wheel And Its Application To Attitude Control in Space. In *Acta Astronautica* **11**(9), 613–619.

[2] Scharfe, M., Meinzer, K. & Zimmermann, R. (1996). Development of a Magnetic-Bearing Momentum Wheel for the AMSAT Phase 3-D Small Satellite. In *International Symposium on Small Satellites*. Annecy, France. No. A97-23887.

[3] Scharfe, M., Roschke, T., Bindl, E., Blonski, D. & Seiler, R. (2001). The Challenges of Miniaturisation For a Magnetic Bearing Wheel. In *Proceedings of the 9th European Space Mechanisms and Tribology Symposium* (Ed. R. A. Harris). Liege, Belgium, 17 – 24.

[4] Gerlach, B., Ehinger, M., Raue, H. K. & Seiler, R. (2005). Gimballing Magnetic Bearing Reaction Wheel With Digital Controller. In *11th European Space Mechanisms and Tribology Symposium, ESMATS 2005* (Ed. B. Warmbein). ESA, Lucerne, Switzerland, 35 – 40.

[5] Sindlinger, R. (1977). Magnetic Bearing Momentum Wheels with Magnetic Gimballing Capability for 3-Axis Active Attitude Control and Energy Storage. In *Attitude and Orbit Control Systems Conference*. European Space Agency, Noordwijk, volume ESA SP-128, 395–401.

[6] D'Arrigo, A. & Rufer, A. (2000). Integrated Electromagnetic Levitation and Guidance System for the Swissmetro Project. In *International Conference on Magnetically Levitated Systems*. Rio de Janeiro, Brazil, 263–268.

[7] Sidi, M. J. (1997). *Spacecraft Dynamics And Control : A Practical Engineering Approach*. Cambridge University Press.

[8] Pechev, A. N. (2007). Feedback-Based Steering Law For Control Moment Gyros. In *Journal of Guidance, Control, and Dynamics* **30**(3), 848–855.

[9] Genta, G. (2005). *Dynamics of Rotating Systems*. Springer, New York.

[10] Bamber, D. C., Palmer, D. P. L. & Mackin, D. S. (2006). Attitude Determination through Image Registration Model and Test-case for Novel Attitude System in Low Earth Orbit. In *AIAA/AAS Astrodynamics Specialists Conference*. Keystone, Colorado, 1–14. No. AIAA 2006-6157.